Alkali-activated slag concrete: fresh and hardened behaviour

F. Puertas[1*], B. González-Fonteboa[2], I. González-Taboada[2], M.M. Alonso[1], M. Torres-Carrasco[1], G. Rojo[2] and F. Martínez-Abella[2]

[1]Eduardo Torroja Institute for Construction Sciences (IETcc-CSIC), C/Serrano Galvache 4, 28033, Madrid, Spain

[2]Department of Construction Technology, University of A Coruña, E.T.S.I. Caminos, Canales, Puertos. Campus Elviña s/n, 15071 La Coruña, Spain

*corresponding author: puertasf@ietcc.csic.es

Abstract

The behaviour of fresh and hardened alkali-activated slag (AAS) and OPC concretes was compared and the effect of mixing time assessed. OPC and AAS concrete slump and rheological results proved to differ, particularly when the slag was activated with waterglass (WG). The nature of the alkaline activator was the key determinant in AAS concrete rheology. Bingham models afforded a good fit to all the OPC and AAS concretes. In OPC and NaOH-activated AAS concretes, longer mixing had an adverse effect on rheology while improving hardened performance only slightly. In WG-AAS concrete, longer mixing times, improved mechanical properties and also rheological behaviour was enhanced, in which those conditions were required to break down the microstructure. Longer mixing raised thixotropy in OPC and NaOH-activated AAS concretes, but lowered the value of this parameter in waterglass-activated slag concrete.

Keywords: rheology, concrete, alkaline activation, blast furnace slag, Bingham model, hardened behaviour

1. Introduction

For over 20 years, the study and development of alkaline activated materials (AAMs), mainly cements and concretes has been the subject of great interest by the scientific community [1–6]. That is largely due to the enormous promise of these products as sustainable alternatives to portland cement-based binders. AAMs are natural or artificial aluminosilicates activated by hydroxide-, silicate- or alkaline carbonate-solutions. Their manufacture not only generates lower GHG (especially CO_2) emissions, but is more economically and environmentally sustainable, for the raw materials or precursors used are often valorised industrial by-products [7–10]. The manufacture of some alkaline activators, sodium silicate or waterglass (WG) especially, also carries adverse environmental impacts, however [11]. The production of possible alternative activators by processing different types of waste (such as glass or rice husk ash) would consequently constitute a further step toward sustainability [12–15] in new binder development.

Alkali-activated slag (AAS) cements and concretes are among the most prominent AAMs, for their manufacture emits ~~73 %~~ less GHGs than portland cement and consumes less energy and water [16]. These AAS systems are also characterised by high mechanical strength and durability [17–22]. ~~They~~ Nonetheless AAS cement, mortar and concretes exhibit two shortcomings that hamper their standardisation and more general use, namely high drying shrinkage [2,23–25] and quick setting when activated with waterglass solutions [26–28].

The reason for such quick setting lies in the initial and speedy formation of a primary C-S-H gel, which hardens sodium silica-activated AAS pastes. Shi and Day [29] used isothermal conduction calorimetry to study slag activation with different activators. They observed two contiguous signals in the pre-induction period in sodium silicate-activated pastes. The first was attributed to slag dissolution and the second to the formation of a primary C-S-H gel as a result of the presence of $[Si0_4]^{4-}$ ions in the solution. This latter signal intensified as the WG silica modulus rose. Primary C-S-H formation was also observed in constant shear rate rheology tests [28,30] on waterglass-activated AAS pastes. After an initial rise, shear declined and flattened, attendant upon paste deflocculation possibly attributable to primary C-S-H flocks gel breakdown. Lengthening mixing time from 3 min to 10 min was also shown to retard initial setting by 40 min and final setting by over 4 h. At a mixing time of 30 min, initial and final settings were also delayed [26].

More recently, the intensity and timing of this rheological signal at constant shear rate in WG-activated AAS pastes have been shown to depend on the Na_2O concentration and the

58 SiO_2/Na_2O modulus in the activating solution used. The higher the latter and consequently the
59 greater the silicon content in the solution, the earlier and more intense the signal [31].

60 Such rapid setting obviously affects rheology and therefore on-site paste and concrete casting.
61 As the literature shows [28,30,31], rheological studies contribute to an understanding of the
62 reasons for such behaviour and the pursuit of possible solutions. Few studies have focused on
63 researching sodium silicate-activated AAS system rheology, however.

64 Palacios et al. [28, 30] found that NaOH-activated AAS pastes fit a Bingham model, whereas
65 WG-activated materials conform to the Herschel-Bulkley model. Studies comparing OPC and
66 AAS rheology based on minislump test-determined workability [31, 32] showed that WG-
67 activated pastes were less workable than NaOH-activated and OPC pastes. Kashani et al. [33],
68 studying hydroxide- and alkaline silicate-activated AAS paste rheology, found that the latter
69 had lower initial shear stress than the former due to the adsorption of silicate ions on the
70 particles, which had a fluidising effect as a result of the increase in the double electrical layer.
71 When these results were studied in conjunction with isothermal conduction calorimetry
72 findings on degree of reaction, the times at which yield stress rose were found to be correlated
73 to the heat release pattern. Those data were consistent with the results reported by Varga et
74 al. [31], where initial yield stress was observed to be lower in WG- than in NaOH-activated AAS
75 pastes. Unlike Varga et al., however, Kashani et al. [33] observed that yield stress was lower in
76 the first 20 min in WG- than in alkaline hydroxide-activated AAS pastes. Different authors may
77 on occasion report contradictory findings due to variations in the activators used and paste
78 mixing history, as well as in the specific rheological study conducted.

79 Fluidity loss has been shown to be greater in sodium silicate-activated AAS mortars than in
80 OPC and NaOH-activated AAS mortars [2,32]. Waterglass-activated AAS mortars have also
81 been found to exhibit lower workability and greater fluidity loss than alkali-activated fly ash
82 mortars [34, 35].

83 Sight should not be lost of the fact that the end product is concrete, however. An
84 understanding of its workability and rheology is consequently of cardinal importance [36,37].
85 Empirical findings such as yielded by the slump test, V-funnel or J-ring [38] not only furnish
86 very valuable information on concrete workability, but can be readily and economically
87 conducted. As operator-sensitive, single-point tests [39,40], they may nonetheless find two
88 very different concretes to be in the same workability class. AAS concrete systems should
89 therefore be studied with multi-point tests that furnish information on rheological parameters
90 such as yield stress, plastic viscosity and information about thixotropy [39–42].

Portland cement concrete rheology has been exhaustively studied and found to fit a Bingham model (Equation 1):

$$\tau = \tau_0 + \mu \cdot \dot{\gamma} \quad (1)$$

where $\dot{\gamma}$ is shear rate (s^{-1}), τ_0 is yield stress (an indication of the force needed to initiate flow) and μ is plastic viscosity (Pa·s) or the material's resistance to flow [40,43]. OPC thixotropy has also been explored by many authors [44–46]. Thixotropy is the property of these systems whereby viscosity gradually declines with rising shear rate and the initial structure is recovered when shear is removed [40,47]. It should not be confounded with the irreversible 'structural breakdown' in cement pastes defined by Tattersall and Banfill [40].

Any number of studies have shown that portland cement concrete rheology, thixotropy and workability vary with the presence of additions [48–50], the presence and composition of superplasticisers [51–53] and the composition and particle size distribution of the aggregates [54–57].

In contrast, rheological studies on alkali-activated concretes are scant to non-existent. The addition of ultrafine fly ash [58] or lime slurry [59] has been observed to improve AAS ~~paste, mortar and~~ concrete workability (lower lost of slump). No information has yet been forthcoming on AAS concrete rheological parameters, however. More specifically, no studies comparing NaOH- or sodium silicate-activated AAS to OPC concrete rheology have been published to date. As noted, moreover, as longer mixing times may induce initial breakdown of the primary C-S-H gel in WG-AAS systems, improving the workability as has been proven in previous studies on AAS paste and mortars [31, 60]. The motivation of this study was to know the effect of longer mixing time of AAS concrete rheology with different alkaline activators (NaOH and Wg) and to compare the results with OPC concretes. Mixing time must be factored into experimental designs to determine NaOH- and WG-activated AAS concrete workability and rheology.

2. Experimental procedure

2.1 Materials

CEM I 52.5 R portland cement (OPC) and ground-granulated blast furnace slag (S) were used as binder to prepare the concretes studied. The chemical composition of these materials was listed in **Table 1** and determined by a PHILIPS PW-1004 X-Ray Fluorescence (XRF) spectroscometer, together with the loss on ignition (found further to European standard EN-

196-2:2014). The ground-granulated blast-furnace slag used in this study had a Blaine specific surface of 346 m^2/kg and a specific gravity of 2,880 kg/m^3. The cement used, the chemical composition for which is given in **Table 1**, had–a Blaine specific surface of 420 m^2/kg and a density of 3,100 kg/m^3. The rolled sand fines had a specific gravity of 2,600 kg/m^3 and an absorption of 0.23 %, both coarse siliceous aggregates had a specific gravity of 2,640 kg/m^3, with 0.36 % absorption in the 4-8 mm material and 0.40 % absorption in the 8-12 mm gravel (**Table 2**). The particle size distribution of the coarse aggregates is shown in **Figure 1**.

Table 1. Chemical composition of blast furnace slag and 52.5R OPC (XRF analysis)

Material	Component (oxide; wt%)										
	SiO_2	Al_2O_3	Fe_2O_3	MnO	MgO	CaO	Na_2O	K_2O	TiO_2	P_2O_5	*LoI
Slag	38.71	10.46	0.33	0.21	7.58	40.62	0.54	0.35	0.37	0.05	-0.30
OPC	19.32	7.90	2.69	0.06	0.81	61.81	0.11	1.02	0.23	0.06	2.90

*LoI = Loss on ignition at 1000 °C

Table 2. Physical properties of natural aggregates

Aggregate	Maximum grain size (mm)	Specific gravity (kg/m^3)	Water absorption (%)
Sand 0-4 mm	4	2,600	0.23
Coarse (4-8 mm)	8	2,640	0.40
Coarse (8-12 mm)	12	2,640	0.36

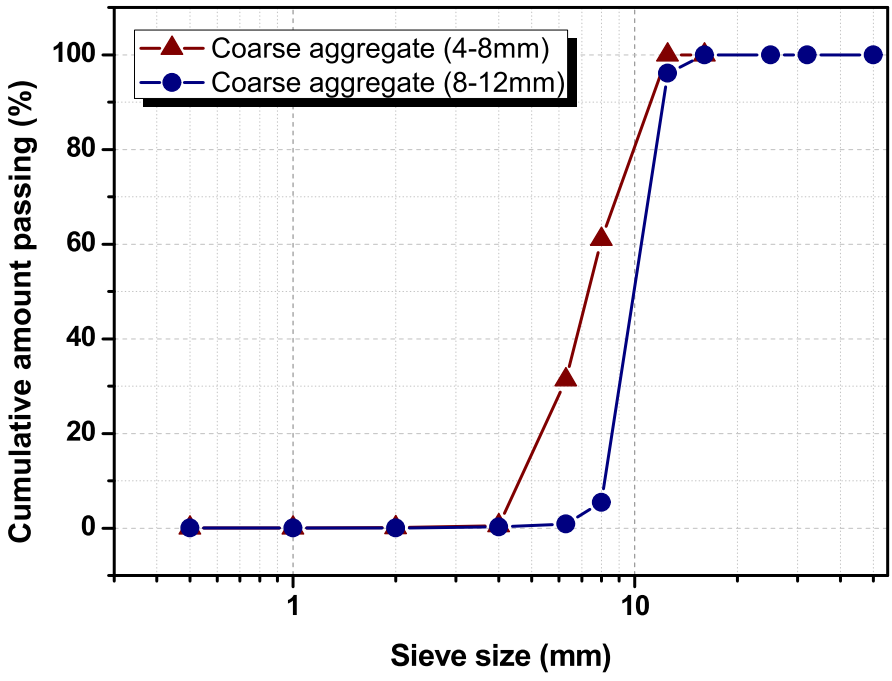

Figure 1. Particle size distribution of coarse aggregates in OPCC and AASC concretes

2.2 Mixture proportions and mixing protocols

The blast furnace slag and cement concretes were designed to a total content of 357 kg/m^3. The OPC concrete was mixed with water and 0.1 % (cement weight) chemical admixture, whereas the alkali-activated slag concretes were mixed with one of two solutions (**Table 3**):

- Panreac 98 % pure, 10 M NaOH (5 % Na_2O by slag mass)
- Sodium silicate hydrate or waterglass (5 % Na_2O by slag mass, SiO_2/Na_2O modulus of 1.2), prepared with Merck sodium silicate (SiO_2: 27 wt%; Na_2O: 8 wt%; H_2O: 65 wt%).

A slump of 120 mm or larger was sought in all cases.

Table 3. Concrete batching (per 1 m^3)

Material (kg)	OPCC	AASC N	AASC WG
Cement	357.0	-	-
Blast furnace slag	-	357.0	357.0
Water	197.5	177.75	145.0
Water in solution	-	19.75	52.5
Fine aggregate	720.5	711.3	563.0
Coarse aggregate 4-8	540.3	533.5	548.0
Coarse aggregate 8-12	540.3	533.5	728.3
L/S	0.55	0.55	0.55
Admixture (wt%)	0.1	-	-
NaOH and sodium silicate	-	23.0	42.5
SiO_2/Na_2O modulus	-	-	1.2
pH solution	7.0	13.6	13.8

Two mixing protocols were deployed to prepare both the OPCC and AASC systems (see **Figure 2**). Protocol 1 corresponds to AAS concrete dosage previously determine in RILEM TC 247-DTA (the stability and good mechanical strenght behaviuor were the main factors considered). In protocol 2 a longer mixing time of all concrete components were considered according to previous rheological studies [26, 31, and 60].

In the first (protocol 1), the aggregates were blended for 2 min in the mixer with 1.65 % of the water. The aggregates were then allowed to stand for 8 min to absorb the mixing water. The binder (portland cement or ground-granulated blast furnace slag) were added and mixed with aggregates during 2 minutes 30 seconds. At this moment, 90% solution (water or alkaline solution) was added and the reference time started when the solution was in contact with the binder. Two minutes later, the rest of the liquid was added, along with the admixtures in the OPCC systems. In this mixing protocol, the mixing time between the aggregates, binder and solution (water or alkaline activator) was 5 minutes. Finally, the mixture is allowed to stand for

2 minutes and again mixed for 2 additional minutes before to start the rheological tests. Entire test lasts 21 minutes 30 seconds (see Figure 2a).

The same stages were followed in protocol 2, although the times varied. The aggregate, binder and liquid were mixed for 11 min rather than 5 min. To maintain the same 21.5 min total time as in protocol 1, that 6 min difference was adjusted as follows: the rest time after blending liquid and aggregate was shortened by 3 min (ending at 7 min), the aggregate-binder blending time by 1 min, the standing time after mixing aggregate, binder and liquid by 1 min and the final mixing time by 1 min (**Figure 2(b)**).

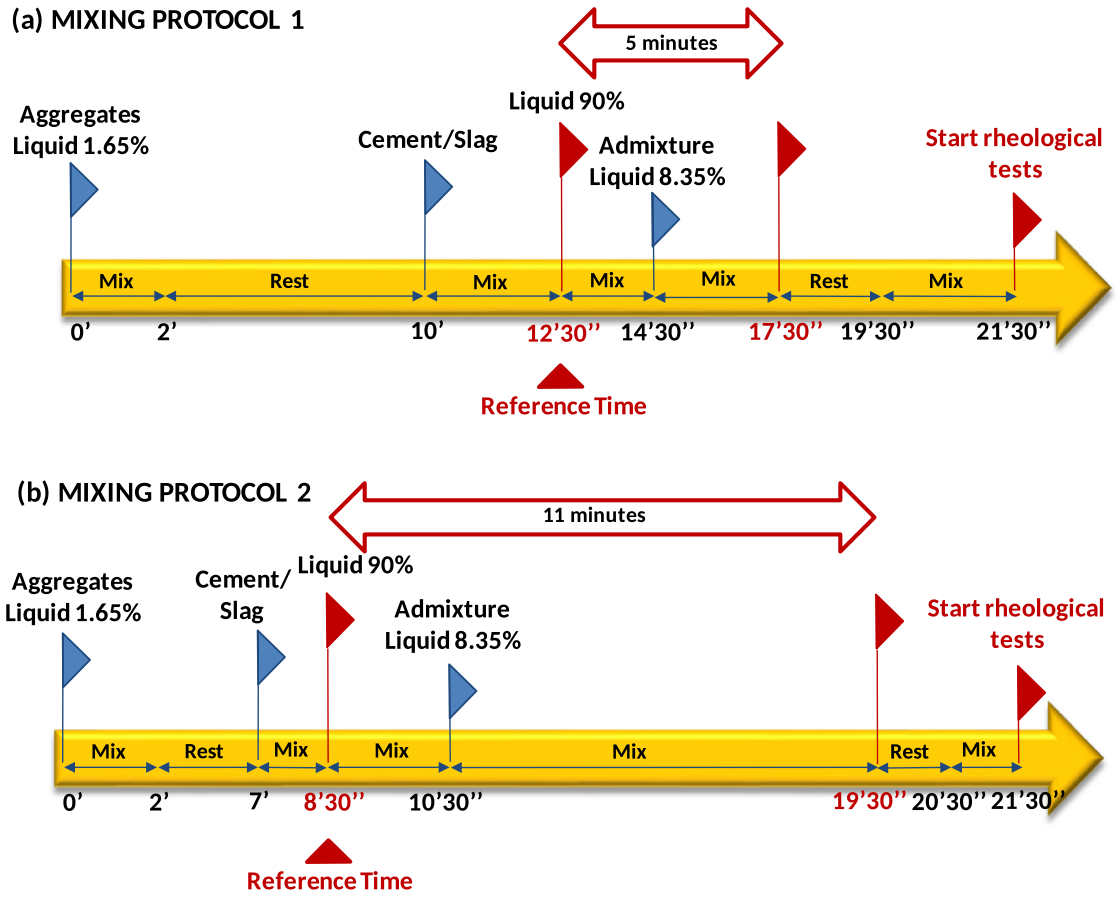

Figure 2. Mixing protocols for OPCC and AASC: **(a)** protocol 1; **(b)** protocol 2; (note differences in mixing and standing times)

Hereinafter, the concretes will be named with a suffix denoting the mixing protocol used.

2.3 Testing program

The slump test described in European standard EN-12350-2 was conducted on all the fresh concretes at each test age. The fresh concrete was also analyzed in an ICAR portable rotational rheometer fitted with a four-bladed vane able to ensure axial symmetry at variable speeds (**Figure 3**). Static (or at-rest) yield stress was determined by stress growth test, while Bingham parameters for dynamic yield stress and plastic viscosity were found by flow curve test method. In this study, rheology tests were performed at 15 min, 30 min, 45 min and 60 min after the liquid was added to the solid.

Figure 3. ICAR rheometer

After the mixing process, part of the concrete was poured from the mixer into the rheometer container. At each testing age, the slump test was carried out. Before beginning this test, the concrete was remixed 30 s. At the same time, the rheological tests were started from the concrete being at rest:

I. The stress growth test started when the vane immersed in the concrete. A constant speed of 0.025 rps was applied as torque was monitored on the computer screen.
II. When peak torque was reached, the vane was removed and the concrete was remixed with a shovel.
III. The vane was reinserted and the flow curve test started. The material rotated at a constant 0.5 rps for 20 s, after which torque was measured at decreasing speeds.

IV. The vane was removed at the end of the test and the concrete was re-shovelled and allowed to stand until the following test time.

The concrete was moulded into 100 mm cubic specimens, demoulded after 24 h and cured in a chamber for 7 d or 28 d, when it was tested for compressive strength as per European standard EN 12390-3. The testing frame was programmed to gradually increase the load at a rate of 0.6±0.2 MPa·s^{-1} to failure.

Cylindrical 150 mm x 200 mm specimens were also prepared for the water permeability test, conducted on the 28 d samples to European standard EN 12390-8. These specimens were placed in a water tank connected to an air compressor fitted with a valve to adjust the pressure, which was applied at 500 kPa (5 bar) for 72 h. They were then tested for splitting tensile strength as per European standard EN 12390-6 and the water penetration depth was measured on the split specimens. Density was found in the fresh concrete as described in European standard EN 12350-6 and density of hardened concrete in the 1 d cured 100 mm concrete cubes as per EN 12390-7.

Total porosity and pore size distribution were found for the 7 d and 28 d specimens on a Micromeritics Autopore IV 9500 mercury intrusion porosimeter.

Hydration was monitored in all systems with a Thermometric TAM Air isothermal conduction calorimeter. The pastes were mixed in a special device fitted with a mechanical stirrer and a syringe to add the liquid to the solids and record the reaction data from the very earliest stages. The liquid/solid ratios used were the same as to prepare the concretes (**Table 3**).

3. Results and discussion

The results obtained for the fresh and hardened concretes are described below.

3.1. Fresh behaviour

The slump values for the OPCC and AAS concretes (AASC N and AASC WG) in **Figure 4(a)** showed that the AASC (and particularly the waterglass-activated) concretes had a larger slump than the OPC concretes.

Similar findings have been reported for mortars [60]. Mixing time was also observed to affect slump, for longer times lowered fluidity in all the mortars. As expected, the slump for OPCC and AASC N declined at longer test times. In the AASC WG concretes, the decline was so steep that it could not be measured at 30 min or 45 min (see **Figure 4(b**). Mixing protocol 2 had a beneficial effect on these concretes, which remained fluid for longer periods.

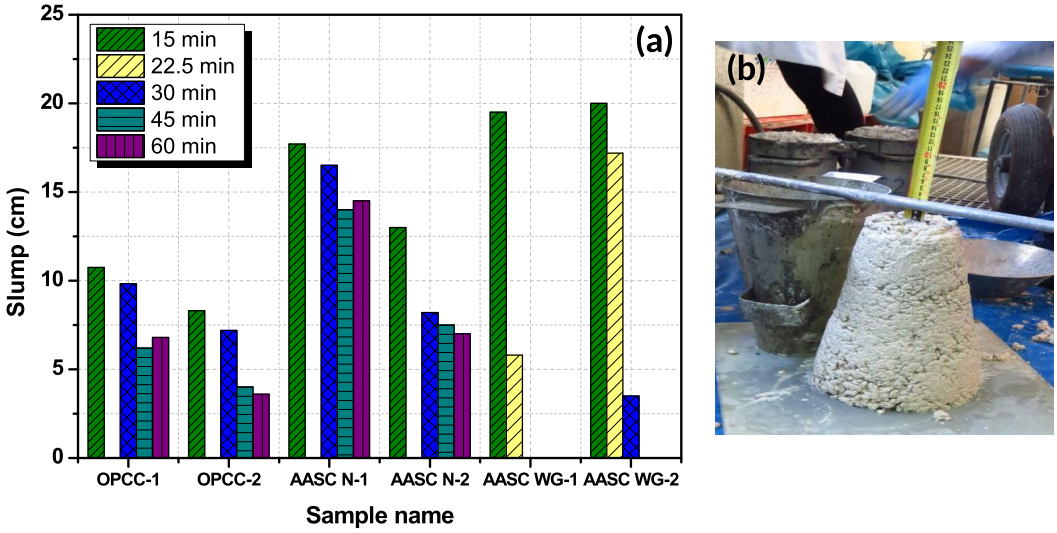

Figure 4. (a) Slump test findings for the concretes studied, where suffix denote the mixing protocol used; **(b)** 22.5 min slump for AASC WG prepared with mixing protocol 1

Different models such as the Herschel-Bulkley model or the modified Bingham model can be considered to describe the behaviour of certain vibrated or self-consolidating concretes. However, as the applied rheological model should be as simple as possible, the Bingham model (Equation 1) for yield stress and plastic viscosity is recommended.

$$\tau = \tau_0 + \mu \cdot \dot{\gamma} \quad (1)$$

Before applying this model, the effect of thixotropy should be verified by checking for torque equilibrium at each rotational velocity on the flow curve, whilst the mix should be examined visually for segregation both during and after the test. These measurements may describe apparently non-linear behaviour due to thixotropy and segregation and should be eliminated [61].

In this study, this possible non-linear behaviour was checked and as it did not occur, in light of the foregoing, the Bingham model was applied, the results of which are shown in **Figure 5** for all the concretes studied.

It can be seen that the standard Bingham model accurately represents all the systems studied, for as the coefficients of determination found for all the curves denoted good correlations. Therefore the flow curves for the concretes studied could be assumed to fit a linear model.

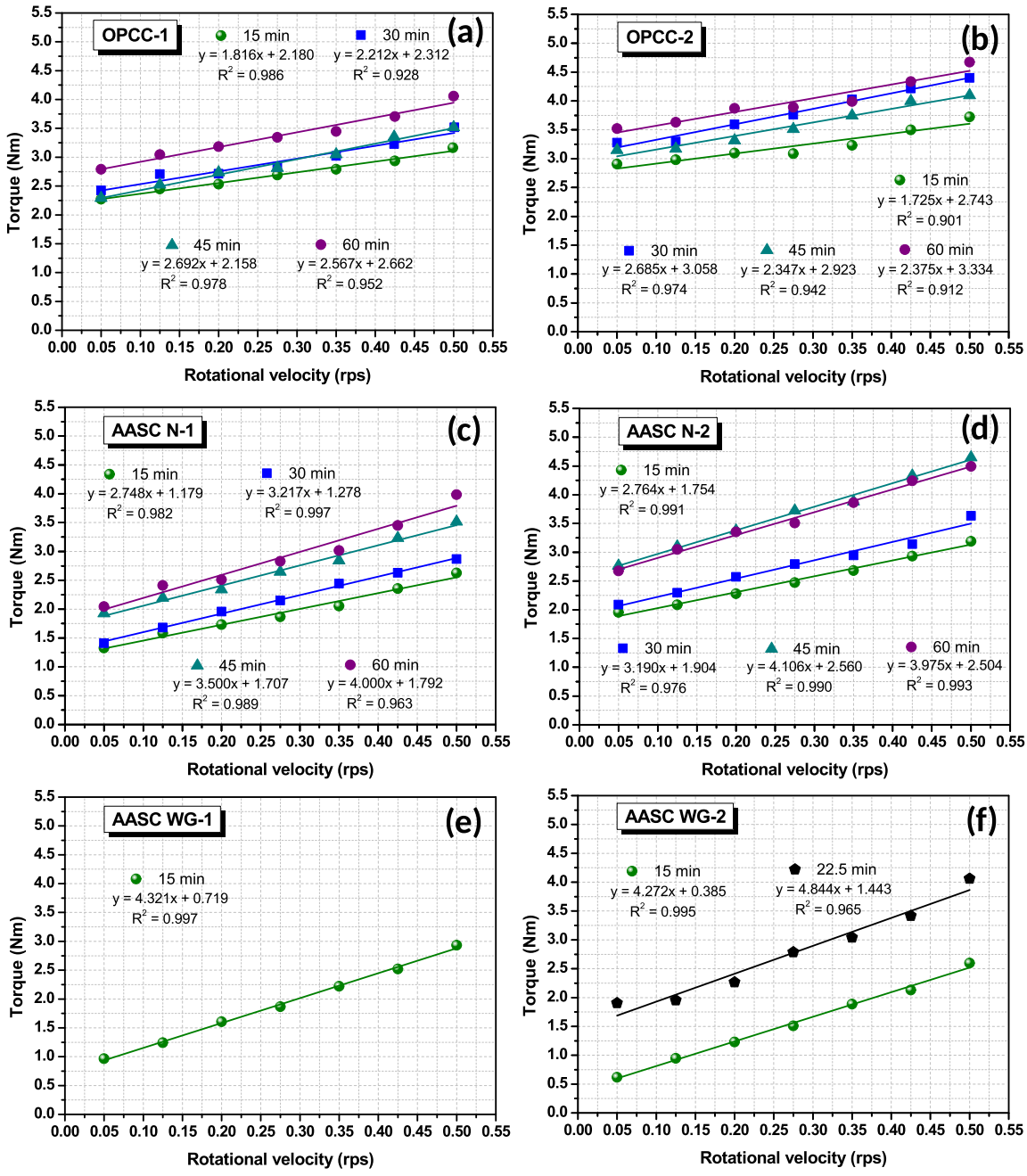

.

Figure 5. ICAR rheometer-determined flow curves for: **(a)** OPCC-1; **(b)** OPCC-2; **(c)** AASC N-1; **(d)** AASC N-2; **(e)** AASC WG-1 and **(f)** AASC WG-2

The standard Bingham model accurately represented all the systems studied, for as the coefficients of determination found for all the curves denoted good correlations~~, the flow curves for the concretes studied could be assumed to fit a linear model.~~

The Reiner-Riwlin equations [62] for the Bingham model were applied to the experimental data to convert the torque-rotational velocity relationship into a shear stress-shear rate relationship, expressed in fundamental units (Pa and Pa·s) (Equations 2 and 3). This procedure transforms a relationship between torque and rotational velocity into a relationship between shear stress and shear rate, expressed in fundamental units (Pa and Pa·s).

$$\tau_0 = \frac{\left(\frac{1}{R_1^2} - \frac{1}{R_2^2}\right)}{4\pi h ln\left(\frac{R_1}{R_2}\right)} G \quad (2)$$

$$\mu_p = \frac{\left(\frac{1}{R_1^2} - \frac{1}{R_2^2}\right)}{4\pi^2 h} H \quad (3)$$

where:

R_1 is the vane radius (m)

R_2 is the outer container radius (m)

h is the vane height (m)

G is the y-intercept on the flow curve (Nm)

H is the slope of the flow curve (Nm·s)

The findings on plastic viscosity and dynamic and static yield stress are shown in **Figure 6**.

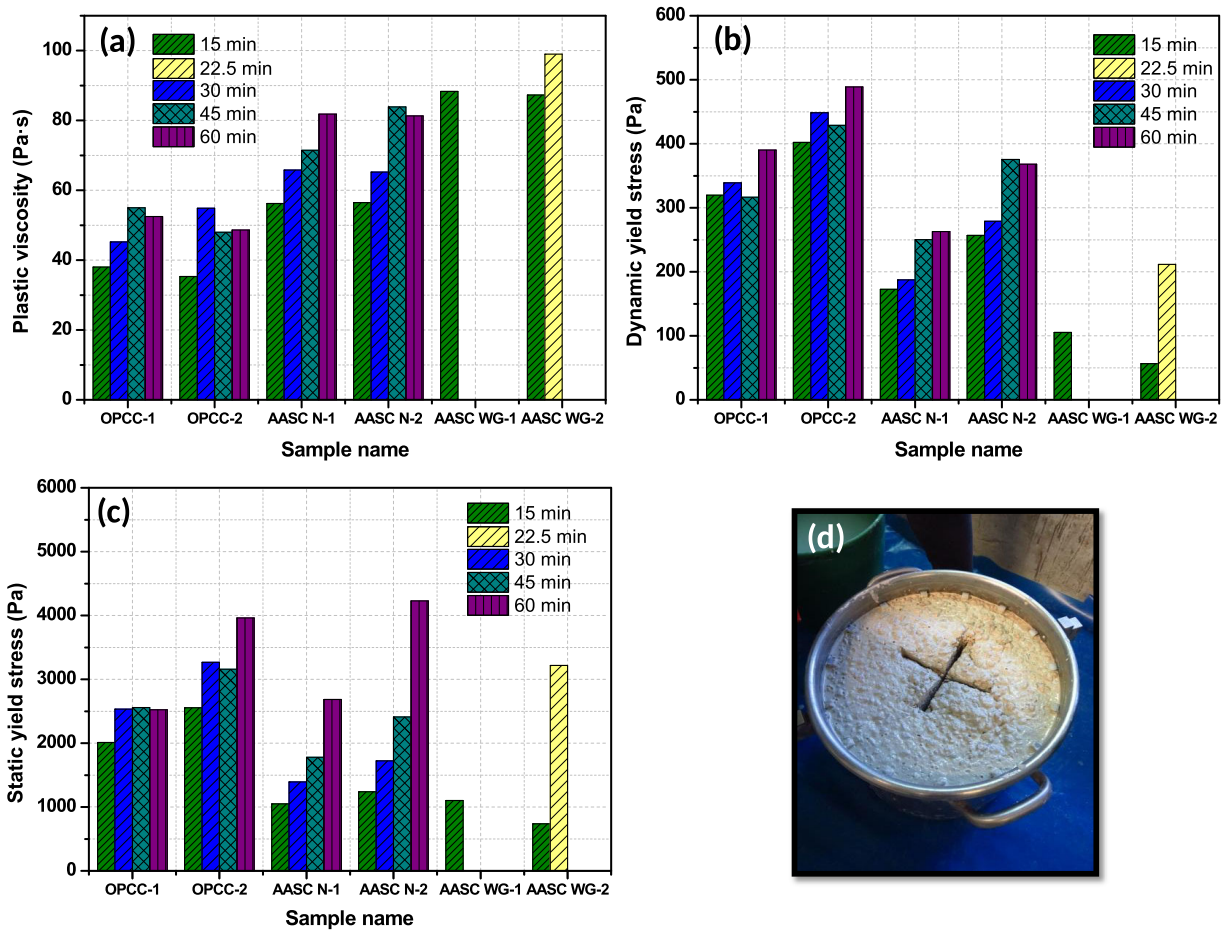

294 **Figure 6. (a)** Plastic viscosity; **(b)** dynamic yield stress; and **(c)** static yield stress for the
295 concretes studied; **(d)** 30 min AASC WG-1

296

297 In the 15 min trials, the OPC concretes exhibited higher static and dynamic yield stress and
298 lower plastic viscosity than the alkali-activate materials. More specifically, the highest yield
299 stress was observed in OPCC -2, although it shared very similar plastic viscosity with OPCC -1.
300 Dynamic yield stress barely rose in the first 45 min in the OPC concretes, and by only 20 %
301 after 60 min, whilst plastic viscosity rose by 40 % after 60 min.

302 The 15 min static and dynamic yield stress values were higher and viscosity was lower in the
303 AASC N than in the AASC WG concretes. The values of these parameters were lowest in
304 protocol 1, sodium hydroxide (N) mixes and somewhat higher in the sodium silicate hydrate
305 (WG) materials mixed to the same protocol. When mixed to protocol 1, the AASC N concretes
306 exhibited 60 min dynamic yield stress 52 % higher than at the outset and 43 % higher when
307 mixed to protocol 2, whilst plastic viscosity grew by 46 % in protocol 1 and 44 % in protocol 2.

These parameters rose so dramatically in protocol 1 AASC WG concretes that the rheological tests could not be conducted after 15 min, or after 22.5 min with protocol 2, at which time the rheological parameters were observed to rise significantly.

Further to the aforementioned findings, longer mixing times raised dynamic yield stress in both OPCC and AASC N. Whilst the mixing protocol did not appear to affect plastic viscosity in OPCC concretes, viscosity rose at later ages when the AASC N mixes were prepared to protocol 2. Longer mixing times improved AASC WG rheology (dynamic yield stress and plastic viscosity).

Some authors describe three mixing stages [63] (**Figure 7**). The first, in which the solid is dispersed in the liquid, is characterised by the transition from initially high inter-particle forces (calling for high mixer power) to a suspension with a significant decline in such forces. The second or optimum stage exhibits asymptotic power demand. It delivers the maximum slump and encompasses the optimal mixing time. Upon finalisation of this stage, inter-particle and particle-mixer collisions may induce wear on the aggregate and cement particles and abrasion in the early hydration products. The result is the third or 'over-mixing' stage, i.e., the appearance of new reaction nuclei that raise rheological parameters and accelerate the decline in workability.

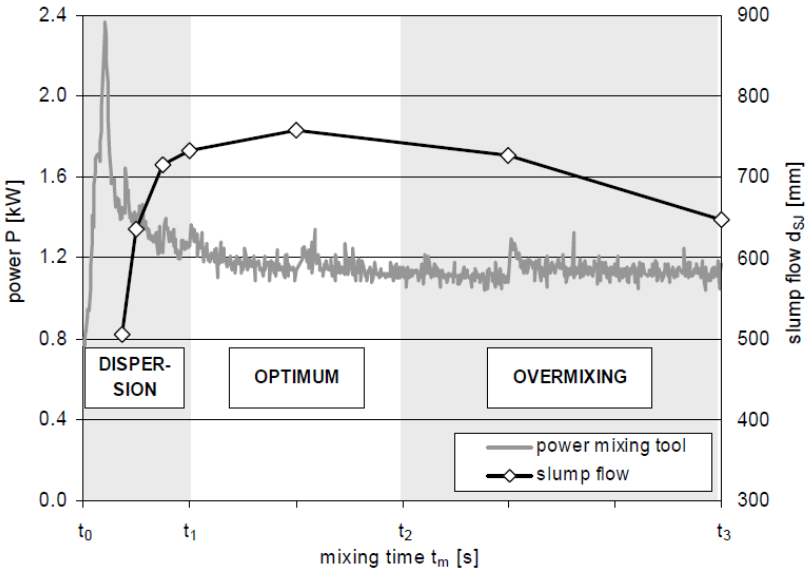

Figure 7. Effect of mixing time [63]

The rise in plastic viscosity and yield stress attendant upon longer mixing times in OPCC and AASC N was indicative of a more compact fresh microstructure. While occasioning over-mixing in these materials, protocol 2 appeared to generate optimum stage conditions in the AASC WG concretes.

As gels seem to be generated at very early ages in AASC WG, longer mixing times would be required to break down the microstructure and improve rheological behaviour in these materials.

When a 15 min at-rest period was used, static yield stress rose by 26 % between 15 min and 30 min in both OPC concretes (**Figure 6(c)**) and remained steady after 45 min (also with 15 min at-rest). After 60 min (15 min at-rest), however, yield stress remained constant under mixing protocol 1 only, rising significantly under protocol 2. In the latter, the over-mixing effect induced by the longer mixing time might have accelerated hydration. These findings infer that the longer mixing protocol prompted significant and irreversible coagulation among cement particles (decline in workability).

Static yield stress rose over time (with a constant 15 min at-rest period) in the concretes activated with either solution. The waterglass-activated samples mixed to protocol 1 could not be tested in the rheometer (for times of over 15 min) due to the high torque generated at the test speed. See **Figure 6(d)** for a photograph of this concrete 30 min after mixing. Static yield stress rose in NaOH-activated concretes mixed to protocol 2 procedures, whereas those same procedures reduced the stress in materials activated with waterglass so effectively that rheological parameters could even be measured after 22.5 min.

The calorimetric findings afforded an explanation for the behaviour induced by protocol 2. Further to those findings (**Figure 8**), heat of hydration declined in the OPC and AAS N pastes at around 20 min-60 min (induction period), i.e., approximately the duration of the rheology tests, an indication that no significant hydration-induced gel formation took place in this stage. In contrast, under the same conditions the AAS WG pastes exhibited a first heat flow peak, attributed to the formation of a C-S-H gel. Gel formation would explain the rheological behaviour of the WG-activated alkaline concretes, which would improve under protocol 2 due to the partial destruction of such primary gels.

Slump values are plotted against dynamic yield stress per density in these concretes in **Figure 9** [64, 65]. The density values are listed in **Table 4**.

An analysis of the data in **Figure 9** showed that both the OPC and AAS concretes, irrespective of the mixing protocol, exhibited similar trends that were, moreover, consistent with the patterns reported in the literature [65]. In other words, the relationship between empirical (slump) and rheological (dynamic yield stress) findings were similar in NaOH- and WG-activated AAS concretes and both were similar to the data for OPC concretes [64, 65].

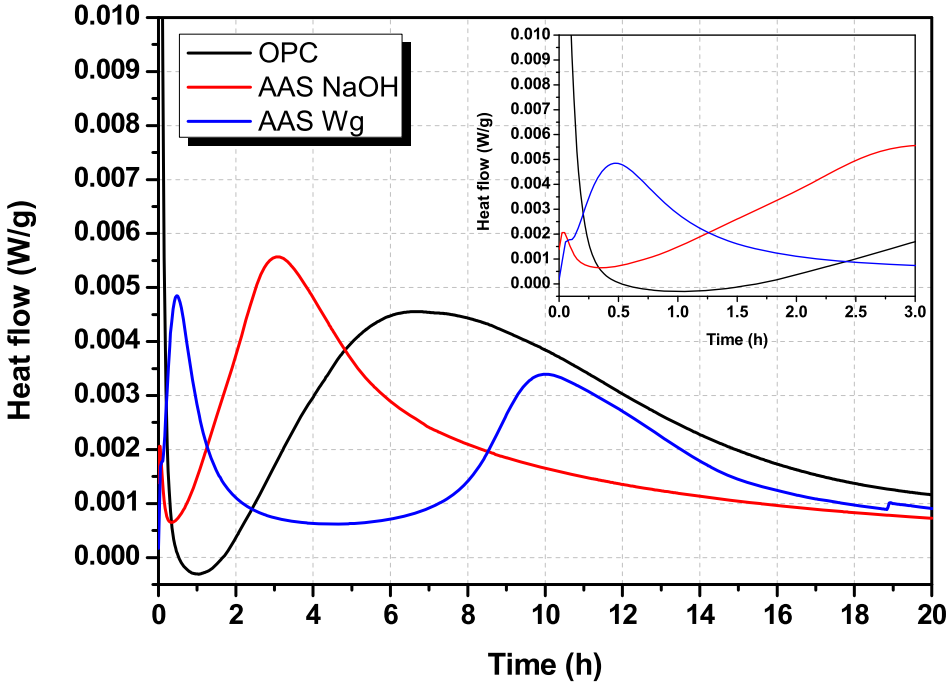

Figure 8. Calorimetric curves for OPC, AAS N and AAS WG pastes

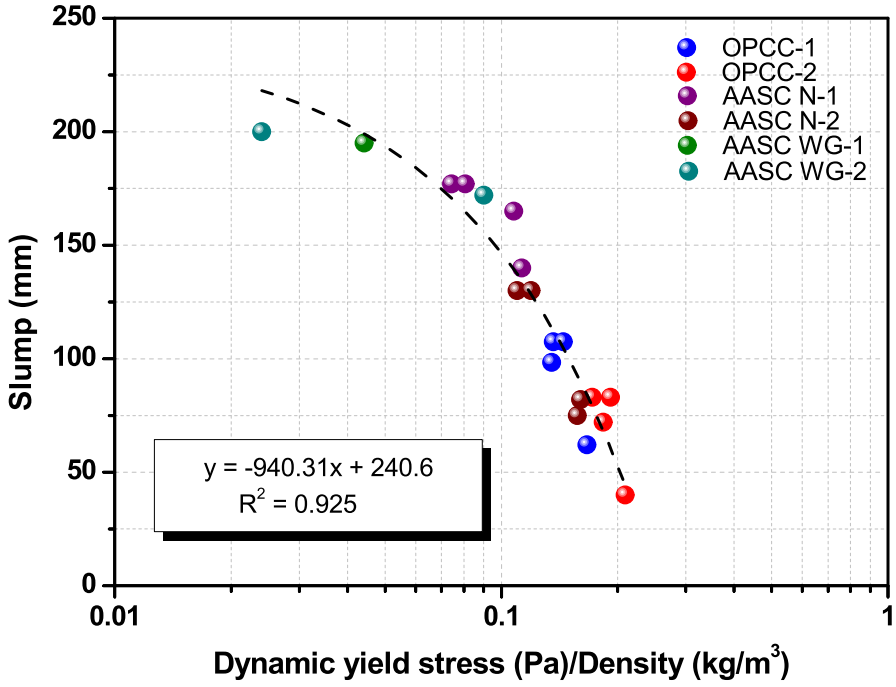

Figure 9. Slump vs dynamic yield stress/density

Concrete thixotropy was assessed as the difference between the peak shear stress and the shear stress at equilibrium in the Stress Growth Test at 30 min (15 min of resting time), except for the AASC WG 2 at 22.5 min (7.5 min of resting time) (see **Figure 10 (a)**). The greater the

difference between peak and equilibrium shear stress, the higher the thixotropy [66-67]. As noted earlier, the test could not be run on AAS WG1 irrespective of the rest time.

The data in **Figure 10(b)** show that longer mixing times generated greater thixotropy in OPCC and AASC N. Those results, which are consistent with the rheological results, can be attributed to the formation of fine particles induced by over-mixing [63, 68]. In contrast, lengthening the mixing time in AASC WG favoured system deflocculation [31], thanks to which the test could be conducted; thixotropy was found to be much higher in this than in the OPC and AASC N systems. At shorter mixing times (protocol 1), which hampered deflocculation, these measurements could not be taken under the protocol conditions established for this study. The findings suggest that longer and perhaps more energetic mixing may have yielded less thixotropic AASC WG concretes.

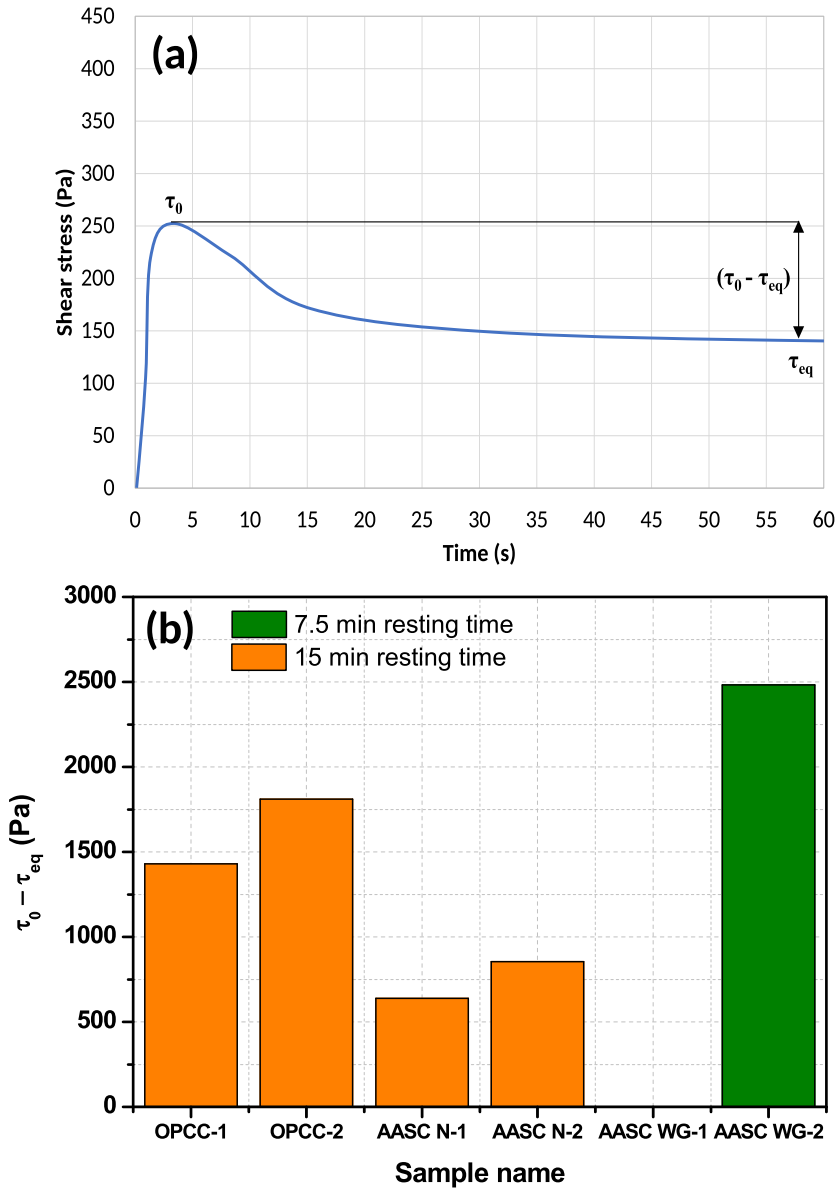

Figure 10. (a) Test protocol; **(b)** peak stress at equilibrium in the concretes

3.2. Hardened behaviour

Figure 11 shows the 7 d and 28 d compressive strength findings for all the concretes, as well as the 28 d total porosity data. The highest strength was observed for the slag concrete alkali-activated with the commercial sodium silicate solution (waterglass), with a 28 d value upward of 60 ± 4.5 MPa. Such performance was comparable to earlier results [20] in which the use of a commercial sodium silicate hydrate (waterglass) induced high strength due to the silicon present in the solution. Lower 28 d strengths, on the order of 16 ± 0.4 MPa, were found when slag was activated with a 5 % Na_2O solution of NaOH. Portland cement exhibited strength 25 %

lower than AASC WG at both ages studied. Mechanical strength appeared to be scantly affected by the mixing protocol used, although when mixed to protocol 2 the materials exhibited slightly higher strength. An increase in mixing time may have favoured reorganisation of the system particles, yielding a somewhat more orderly and compact microstructure that would explain these findings.

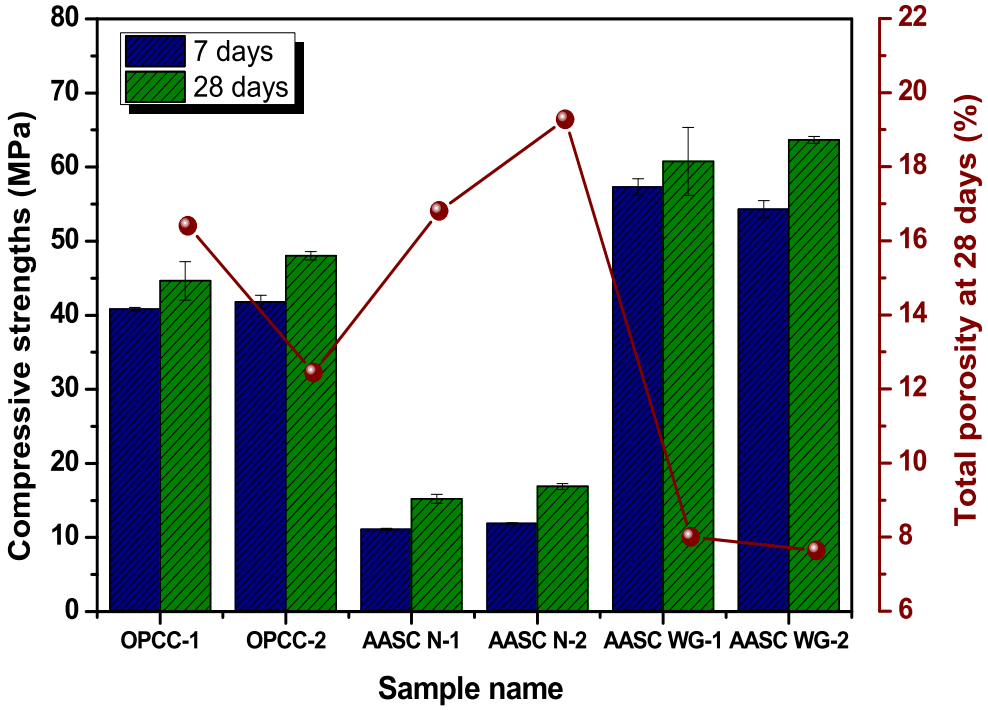

Figure 11. 7 and 28 d compressive strength and 28 d total porosity

The strength findings were related to the total porosity (shown as per cent of total sample volume), density and water permeability data shown in **Table 4**.

Table 4. 28 d water permeability front, total porosity (%) and density in the concretes studied

Concrete	Water Permeability front (mm)	Total porosity (%)	Fresh density (kg/m³)	Hardened density (kg/m³)
OPCC -1	11.0	16.4	2,342.7	2,359.4
OPCC -2	6.8	12.4	2,337.9	2,362.2
AASC N-1	11.0	16.8	2,325.3	2,371.1
AASC N-2	9.5	19.3	2,339.7	2,366.5
AASC WG-1	0	8.0	2,385.8	2,406.6
AASC WG-2	0	7.6	2,348.8	2,390.1

The NaOH-activated slag concretes had 16 %-20 % total porosity, whereas the lower total porosity (7 %-8 %) in the sodium silicate-activated materials was attributed to the presence of silicon in the medium. These total porosity data were directly related to the compressive strength values observed. Total porosity was not as low in portland cement as expected on the grounds of its mechanical strength, however. The explanation lies in the microstructural differences (due to the formation of different hydration products) in alkali-activated and portland cement concretes that determine the way the cementitious matrices bond to the aggregates. In alkali-activated systems, aggregate and cementitious matrix bond well, affording these systems high mechanical stability [20].

Another explanation for the difference in mechanical performance between alkali-activated and portland cement concretes lies in the difference in their respective hydration products: C-A-S-H and C-S-H gels. The main product of blast furnace slag activation is a calcium aluminosilicate hydrate (C-A-S-H) gel, similar to the gel generated in ordinary portland cement hydration, but with a lower Ca/Si ratio, which generally ranges from 0.9 to 1.2 [69-73]. When the activator used is a sodium silicate hydrate (waterglass), the silicon present in the activating solution, and consequently in the system, induces a decline in the Ca/Si ratio to around 0.8. That in turn prompts the formation of longer mean chain lengths and structures comparable to tobermorites [72], yielding an end product that exhibits high mechanical strength and the low porosity required to ensure durability.

Further to the water penetration data (**Table 4**), permeability front depths were similar in the OPCC and AASC N systems, and slightly shallower with protocol 2 than with protocol 1, a finding consistent with the strength data. Longer mixing times yielded higher strength and durability. Water failed to penetrate the AASC WG systems, an observation likewise consistent with the mechanical behaviour observed. In these systems, the silicon sourced from the activating solution induced the formation of longer gels, which would account for the low porosity of the final products.

Fresh and hardened concrete density data are shown in **Table 4**. The AASC WG concretes were the densest and most compact in both states. These concretes are known to exhibit a very compact microstructure [72]. The longer mixing time (protocol 2) appeared to have a beneficial effect on these concretes. In OPCC and AASC N, which exhibited similar and lower densities, the mixing procedure appeared to have less of an impact than in (especially the fresh) AASC WG concretes.

The mixing protocol appeared to affect concrete rheology more than its strength. In AASC WG, both rheological and mechanical behaviour improved at longer mixing times. Mixing protocol 2 had an adverse effect on OPCC and AASC N rheology, while improving the performance of the hardened materials only slightly.

4. Conclusions

The main conclusions obtained from this study are:

- The slump and rheological behaviour of OPCC and AASC differed, particularly where AASC was activated with waterglass. It has been demonstrated that the nature of the alkaline activator is the key determinant in AAS concrete rheology. For first time has been proved that the relationship between the empirical and rheological parameters in OPCC and AASCC followed a similar pattern, which was likewise similar to the trend identified in the literature for OPC systems.
- Bingham models afforded a good fit to all the OPCC and AASC studied.
- Longer mixing times had an adverse effect on dynamic and static yield stress and prompted significant and irreversible coagulation among cement particles (decline in workability) in OPC and AAS N concretes. In contrast, longer mixing times were favourable in AAS WG concrete, in which they would be required to break down the microstructure to enhance rheological behaviour. These results proved that for AAS Wg concrete preparation is recommended to longer mixing time. That would have effect on future standardization of these eco-efficient building materials.
- Thixotropy rose in OPC and AAS N concretes with mixing time, whereas in AASC WG the opposite was observed. The findings reported hereunder showed that in waterglass-activated AAS concretes, longer or more energetic mixing would yield less thixotropic materials.
- The mixing protocol also appeared to affect concrete rheology (fresh behaviour) more than its strength (hardened behaviour). In AASC WG, both rheological and mechanical behaviour improved at longer mixing times. Mixing protocol 2 had an adverse effect on OPCC and AASC N rheology, while improving the performance of the hardened materials only slightly.

5. Acknowledgments

This study was funded by the Spanish Ministry of the Economy under Projects BIA2013-47876-C2-1-P and BIA2014-58063-R.

6. References

[1] Y. Luna-Galiano, C. Fernández-Pereira, M. Izquierdo, ontributions to the study of porosity in fly ash-based geopolymers. Relationship between degree of reaction, porosity and compressive strength, Mater. Construcc. 66 [324] (2016) e098.

[2] F. Pacheco-Torgal, J.A. Labrincha, C. Leonelli, A. Palomo, P. Chindaprasirt, Handbook of Alkali-activated cements, mortars and concretes, Woodhead Publishing series in civil and structural engineering, 2015.

[3] C. Shi, P. Krivenko, D. Roy, Alkali-Activated Cements and Concretes, Taylor and Francis, London and New York, 2006.

[4] M.C.G. Juenger, F. Winnefeld, J.L. Provis, J.H. Ideker, Advances in alternative cementitious binders, Cem. Concr. Res. 41 (2011) 1232–1243.

[5] J.L. Provis, A. Palomo, C. Shi, Advances in understanding alkali-activated materials, Cem. Concr. Res. 78 (2015) 110–125.

[6] B. Singh, G. Ishwarya, M. Gupta, S.K. Bhattacharyya, Geopolymer concrete: A review of some recent developments, Constr. Build. Mater. 85 (2015) 78–90.

[7] C. Shi, A. Jiménez-Fernández, A. Palomo, New cements for the 21st century: The pursuit of an alternative to Portland cement, Cem. Concr. Res. 41 (2011) 750–763.

[8] J.S.J. Van Deventer, J.L. Provis, P. Duxson, Technical and commercial progress in the adoption of geopolymer cement, Miner. Eng. 29 (2012) 89–104.

[9] J.L. Provis, Geopolymers and other alkali activated materials: why, how, and what?, Mater. Struct. 47 (2014) 11–25.

[10] A.F. Abdalqader, F. Jin, A. Al-Tabbaa, Development of greener alkali-activated cement: Utilisation of sodium carbonate for activating slag and fly ash mixtures, J. Clean. Prod. 113 (2016) 66–75.

[11] A.S. Brykov, V.I. Korneev, Production and usage of powdered alkali metal silicate hydrates, Metallurgist. 52 (2009) 648–652.

[12] F. Puertas, M. Torres-Carrasco, Use of glass waste as an activator in the preparation of

alkali-activated slag. Mechanical strength and paste characterisation, Cem. Concr. Res. 57 (2014) 95–104.

[13] J.M. Mejía, R. Mejía de Gutiérrez, F. Puertas, Rice husk ash as a source of silica in alkali-activated fly ash and granulated blast furnace slag systems, Mater. Construcc. 63 [311] (2013) 361–375.

[14] M. Torres-Carrasco, F. Puertas, Waste glass in the geopolymer preparation. Mechanical and microstructural characterisation, J. Clean. Prod. 90 (2015) 397–408.

[15] M.A. Villaquirán-Caicedo, R. Mejía de Gutiérrez, N.C. Gallego A novel Mk-based geopolymer composite activated with rice husk ash and KOH: performance at high temperature, Mater. Construcc. 67 [326] (2017). e117.

[16] M. Jiang, X. Chen, F. Rajabipour, A.M. Asce, C.T. Hendrickson, D.M. Asce, Comparative Life Cycle Assessment of Conventional , Glass Powder , and Alkali-Activated Slag Concrete and Mortar, J. Infrastruct. Syst. 20 (2014).

[17] A. Fernández-Jiménez, J.G. Palomo, F. Puertas, Alkali-activated slag mortars Mechanical strength behaviour, Cem. Concr. Compos. 29 (1999) 1313–1321.

[18] S. Aydın, B. Baradan, Effect of activator type and content on properties of alkali-activated slag mortars, Compos. Part B Eng. 57 (2014) 166–172.

[19] F. Puertas, R. Gutiérrez, A. Fernández-Jiménez, S. Delvasto, J. Maldonado Alkaline cement mortars. Chemical resistance to sulfate and seawater attack, Mater. Construcc.. 52 [267] (2002) 55–71.

[20] M. Torres-Carrasco, M. Tognonvi, A. Tagnit-Hamou, F. Puertas, Durability of Alkali-Activated Slag Concretes Prepared using waste glass as Alternative activator, ACI. 112 (2015) 791–800.

[21] M. Chi, Effects of dosage of alkali-activated solution and curing conditions on the properties and durability of alkali-activated slag concrete, Constr. Build. Mater. 35 (2012) 240–245.

[22] A.M. Rashad, A comprehensive overview about the influence of different additives on the properties of alkali-activated slag - A guide for Civil Engineer, Constr. Build. Mater. 47 (2013) 29–55.

[23] C. Duran Atiş, C. Bilim, Ö. Çelik, O. Karahan, Influence of activator on the strength and drying shrinkage of alkali-activated slag mortar, Constr. Build. Mater. 23 (2009) 548–

555.

[24] M. Palacios, F. Puertas, Effect of shrinkage-reducing admixtures on the properties of alkali-activated slag mortars and pastes, Cem. Concr. Res. 37 (2007) 691–702.

[25] H. Ye, A. Radllinska, Shrinkage mechanisms of alkali-activated slag, Cem. Concr. Res. 88 (2016) 126–135.

[26] M.Palacios, F. Puertas. Effectivenss of mixing time on hardened properties of waterglass-activated slag pastes and mortars. ACI Materials, n° 108 (2011), 73-78.

[27] A. Fernandez-Jimenez, F. Puertas, Setting of alkali-activated slag cement. Influence of activator nature, Adv. Cem. Res. 13 (2001) 115–121.

[28] M. Palacios, P. Banfill, F. Puertas, Rheology and setting of alkali-activated slag pastes and mortars: Effect of organic admixture, ACI Mater. J. 105 (2008) 140–148.

[29] C. Shi, R.L. Day, A calorimetric study of early hydration of alkali-slag cements, Cem. Concr. Res. 25 (1995) 1333–1346.

[30] M. Palacios, Empleo de aditivos orgánicos en la mejora de las propiedades de cementos y morteros de escoria activada alcalinamente PhD Tesis UAM Madrid, Spain, 2006.

[31] F. Puertas, C. Varga, M.M. Alonso, Rheology of alkali-activated slag pastes. Effect of the nature and concentration of the activating solution, Cem. Concr. Compos. 53 (2014) 279–288.

[32] M. Palacios, F. Puertas, Effect of superplastisizer and shrinkage reducing admixtures on alkali-activated slag pastes and mortars, Cem. Concr. Res. 35 (2005) 1358–1367.

[33] A. Kashani, J.L. Provis, G.G. Qiao, J.S.J. Van Deventer, The interrelationship between surface chemistry and rheology in alkali activated slag paste, Constr. Build. Mater. 65 (2014) 583–591.

[34] K.-H. Yang, J.-K. Song, A.F. Ashour, E.-T. Lee, Properties of cementless mortars activated by sodium silicate, Constr. Build. Mater. 22 (2008) 1981–1989.

[35] C. Varga. Cementos activados alcalinamente: Comportamiento reológico y durable en medio ácido. PhD Tesis UNED Madrid, Spain, 2015

[36] K. Kovler, N. Roussel, Properties of fresh and hardened concrete, Cem. Concr. Res. 41 (2011) 775–792.

[37] S. Amziane, C.F. Ferraris, E.P. Koehler, Measurement of Workability of Fresh Concrete

605 Using a Mixing Truck Sofiane Amziane, Chiara F. Ferraris, Eric P. Koehler, J. Res. Natl.
606 Inst. Stand. Technol. 110 (2005) 55–66.

607 [38] E.P. Koehler, D.W. Fowler, Summary of Concrete Workability Test Methods, (2003) 92.

608 [39] O.H. Wallevik, J.E. Wallevik, Rheology as a tool in concrete science: The use of
609 rheographs and workability boxes, Cem. Concr. Res. 41 (2011) 1279–1288.

610 [40] G.H. Tattersall, P. Banfill, The Rheology of Fresh Concrete, Pitman Books Limited, Great
611 Britain, 1983.

612 [41] M. Greim, Equipos y sistemas para el control de calidad de hormigones, morteros y
613 áridos, Cem. Y Hormigón. 99 (2009) 34–38.

614 [42] P. Estell'e, C. Lanos, High torque vane rheometer for concrete: principle and validation
615 from rheological measurements, Appl. Rheol. 22 (2012) 12881.

616 [43] F. Mahmoodzadeh, S.E. Chidiac, Rheological models for predicting plastic viscosity and
617 yield stress of fresh concrete, Cem. Concr. Res. 49 (2013) 1–9.

618 [44] N. Roussel, A thixotropy model for fresh fluid concretes: Theory, validation and
619 applications, Cem. Concr. Res. 36 (2006) 1797–1806.

620 [45] N. Roussel, G. Ovarlez, S. Garrault, C. Brumaud, The origins of thixotropy of fresh
621 cement pastes, Cem. Concr. Res. 42 (2012) 148–157.

622 [46] Y. Tan, G. Cao, H. Zhang, J. Wang, R. Deng, X. Xiao, B. Wu, Study on the thixotropy of
623 the fresh concrete using DEM, Procedia Eng. 102 (2015) 1944–1950.

624 [47] J.E. Wallevik, Thixotropic investigation on cement paste: Experimental and numerical
625 approach, J. Nonnewton. Fluid Mech. 132 (2005) 86–99.

626 [48] P. Ghoddousi, A.A. Shirzadi Javid, J. Sobhani, Effects of particle packing density on the
627 stability and rheology of self-consolidating concrete containing mineral admixtures,
628 Constr. Build. Mater. 53 (2014) 102–109.

629 [49] O. Boukendakdji, S. Kenai, E.H. Kadri, F. Rouis, Effect of slag on the rheology of fresh
630 self-compacted concrete, Constr. Build. Mater. 23 (2009) 2593–2598.

631 [50] A.A.A. Hassan, M. Lachemi, K.M.A. Hossain, Effect of metakaolin on the rheology of self-
632 consolidating concrete., in: Des. Prod. Place. Self Consol. Concr. RILEM State Art
633 Reports, 2010: pp. 103–112.

634 [51] A. Lange, T. Hirata, J. Plank, Influence of the HLB value of polycarboxylate

635 superplasticizers on the flow behavior of mortar and concrete, Cem. Concr. Res. 60
636 (2014) 45–50.

637 [52] A. Mardani-Aghabaglou, M. Tuyan, G. Yilmaz, Ö. Ariöz, K. Ramyar, Effect of different
638 types of superplasticizer on fresh, rheological and strength properties of self-
639 consolidating concrete, Constr. Build. Mater. 47 (2013) 1020–1025.

640 [53] R. Flatt, I. Schober, Superplasticizers and the rheology of concreteR. Flatt, I. Schober//,
641 in: Underst. Rheol. Concr., 2012: pp. 144–208.

642 [54] F. Cartuxo, J. De Brito, L. Evangelista, J.R. Jiménez, E.F. Ledesma, Rheological behaviour
643 of concrete made with fine recycled concrete aggregates - Influence of the
644 superplasticizer, Constr. Build. Mater. 89 (2015) 36–47.

645 [55] L. Evangelista, J. De Brito, Concrete with fine recycled aggregates: a review, Eur. J.
646 Environ. Civ. Eng. 18 (2013) 129–172.

647 [56] D. Carro-López, B. González-Fonteboa, J. De Brito, F. Martínez-Abella, I. González-
648 Taboada, P. Silva, Study of the rheology of self-compacting concrete with fine recycled
649 concrete aggregates, Constr. Build. Mater. 96 (2015) 491–501.

650 [57] R. Cepuritis, S. Jacobsen, B. Pedersen, E. Mørtsell, Crushed sand in concrete - Effect of
651 particle shape in different fractions and filler properties on rheology, Cem. Concr.
652 Compos. 71 (2016) 26–41.

653 [58] F. Collins, J.G. Sanjayan, Effects of ultra-fine materials on workability and strength of
654 concrete containing alkali-activated slag as the binder, Cem. Concr. Res. 29 (1999) 459–
655 462.

656 [59] F.G. Collins, J.G. Sanjayan, Workability and mechanical properties of alkali activated slag
657 concrete, Cem. Concr. Res. 29 (1999) 455–458.

658 [60] M.M. Alonso, S. Gismera, M.T. Blanco, M. Lanzón, F. Puertas. Alkali-activated mortars:
659 workability and rheological behaviour, 145 (2017) 576-587

660 [61] O.H. Wallevik, D.Feys, J.E. Wallevik, K. Khayat Avoiding inaccurate interpretations of
661 rheological measurements for cement-based materials Cem. Concr. Res, 78, (2015),
662 100-109.

663 [62] D.Feys, J.E. Wallevik,A. Yahia, K.H. Khayat, O.H. Wallevik. Extension of the Reiner–Riwlin
664 equation to determine modified Bingham parameters measured in coaxial cylinders
665 rheometers Mat. Struct. 46,(2013), 289-311.

[63] D. Lowke, P. Schiessl. Effect of Mixing Energy on Fresh Properties of SCC SCC2005, in: Proc 4th Int RILEM Symp Self-Compacting Concr Chicago, 2005, 2

[64] N. Roussel, C. Stefani, R. Leroy. From mini-cone test to Abrams cone test: measurement of cement-based materials yield stress using slump tests. Cem. Concr. Res.35, [5] (2005) 817-822.

[65] N. Roussel. Correlation between Yield Stress and Slump: Comparison between Numerical Simulations and Concrete Rheometers Results. Materials and Structures. 39 (2006) 501-509.

[66] J. Assaad. Formwork pressure of self consolodating concrete - Influence of thixotropy. PhD Dissertation, University of Sherbrooke, Canada, 2004

[67] I. González Taboada. Self compacting recycled concrete: basic mechanical properties, rheology, robutness and thixotropy. PhD Dissertation, University of A Coruña, Spain, 2017

[68] M.K. Rahman, M.H. Baluch, M.A. Malik. Thixotropic behavior of self compacting concrete with different mineral admixtures. Constrcc. Buid. Mat. 50 (2014) 710-717.

[69] S.D. Wang, X.C. Pu, K.L. Scrivener, P.L. Pratt, Alkali-activated slag cement and concrete: a review of properties and problems, Adv. Cem. Res. 7 (1995) 93–102.

[70] S. Wang, K.L. Scrivener, Hydration products of alkali activated slag cement, Cem. Concr. Res. 25 (1995) 561–571.

[71] A. Fernández-Jiménez, F. Puertas, Structure of Calcium Silicate Hydrates Formed in Alkaline-Activated Slag : Influence of the Type of Alkaline Activator, J. Am. Ceram. Soc. 86 (2003) 1389–1394.

[72] F. Puertas, M. Palacios, H. Manzano, J.S. Dolado, a. Rico, J. Rodríguez, A model for the C-A-S-H gel formed in alkali-activated slag cements, J. Eur. Ceram. Soc. 31 (2011) 2043–2056.

[73] R.J. Myers, S. a Bernal, R. San Nicolas, J.L. Provis, Generalized structural description of calcium-sodium aluminosilicate hydrate gels: the cross-linked substituted tobermorite model., Langmuir. 29 (2013) 5294–306.